2008

# Mutational Analysis of the Stability of the H2A and H2B Histone Monomers

Matthew R. Stump
*George Fox University*, mstump@georgefox.edu

Lisa M. Gloss
*Washington State University*

# Mutational Analysis of the Stability of the H2A and H2B Histone Monomers


## Matthew R. Stump and Lisa M. Gloss*

*School of Molecular Biosciences, Washington State University, Pullman, WA 99164-4660, USA*



*Received 27 August 2008; received in revised form 8 October 2008; accepted 9 October 2008*
Available online 21 October 2008



The eukaryotic histone heterodimer H2A–H2B folds through an obligatory dimeric intermediate that forms in a nearly diffusion-limited association reaction in the stopped-flow dead time. It is unclear whether there is partial folding of the isolated monomers before association. To address the possible contributions of structure in the monomers to the rapid association, we characterized H2A and H2B monomers in the absence of their heterodimeric partner. By far-UV circular dichroism, the H2A and H2B monomers are 15% and 31% helical, respectively—significantly less than observed in X-ray crystal structures. Acrylamide quenching of the intrinsic Tyr fluorescence was indicative of tertiary structure. The H2A and H2B monomers exhibit free energies of unfolding of 2.5 and 2.9 kcal $mol^{-1}$, respectively; at 10 μM, the sum of the stability of the monomers is ~60% of the stability of the native dimer. The helical content, stability, and *m* values indicate that H2B has a more stable, compact structure than H2A. The monomer *m* values are larger than expected for the extended histone fold motif, suggesting that the monomers adopt an overly collapsed structure. Stopped-flow refolding—initiated from urea-denatured monomers or the partially folded monomers populated at low denaturant concentrations—yielded essentially identical rates, indicating that monomer folding is productive in the rapid association and folding of the heterodimer. A series of Ala and Gly mutations were introduced into H2A and H2B to probe the importance of helix propensity on the structure and stability of the monomers. The mutational studies show that the central α-helix of the histone fold, which makes extensive inter-monomer contacts, is structured in H2B but only partially folded in H2A.





*Keywords:* equilibrium stability; kinetic intermediates; circular dichroism; fluorescence; ϕ values

***Edited by C. R. Matthews***



*Corresponding author. E-mail address: lmgloss@wsu.edu.


Abbreviations used: α1, α2, and α3, the first, second, and third helices, respectively, of the canonical histone fold; αC, the C-terminal helices of H2A and H2B beyond the canonical histone fold; $C_M$, the concentration of urea at the midpoint of the equilibrium unfolding transition; ΔASA, change in solvent accessible surface area between the native and unfolded species; $\Delta G°(H_2O)$, the free energy of unfolding in the absence of denaturant; $F_{app}$, apparent fraction of unfolded monomer; FIS, *E. coli* Factor for Inversion Stimulation; FL, fluorescence; $I_2$, dimeric folding intermediate; KPi, potassium phosphate, pH7.2; $K_2$EDTA, dipotassium ethylenediaminetetraacetic acid; *m* value, parameter describing the sensitivity of the unfolding transition to the [Urea]; 2M, two dissociated, partially folded monomers; MRE, mean residue ellipticity, normalization of CD data for protein concentration and number of residues; $N_2$, native dimer; NCP, nucleosome core particle; SEC, size-exclusion chromatography; SF, stopped flow; TMAO, trimethylamine-*N*-oxide; TR, Trp repressor; 2U, two unfolded, dissociated monomers.

## Introduction

In contrast to monomeric proteins, the folding pathways of oligomers are complicated by folding codes written within multiple polypeptide chains. Traversing the oligomeric folding energy landscape involves the formation of secondary and tertiary structure coordinated with the appropriate intermolecular associations to achieve the native quaternary state. Small dimers (<60 residues per monomer) can fold via a single, second-order kinetic phase (e.g., the homodimeric bacteriophage P22 Arc repressor[1] and coiled coils, such as the GCN4 leucine zipper peptides).[2–4] Larger, multidomain, oligomeric systems exhibit complex folding mechanisms, including kinetic intermediates and parallel pathways (for review, see Ref. 5). Population of kinetic intermediates is especially significant because association of

partially folded species is often a prerequisite for aggregation and fibrillation.[6]

The biophysical characterization of partially folded intermediates provides insight into the rules by which amino acid sequences encode the structure and stability of the native fold.[7] Defining the thermodynamic properties of the oligomerization-competent species is an important step in understanding how appropriate protein–protein interactions are formed rapidly. Because of their transient nature, characterization of kinetic intermediates is inherently difficult. Trapping partially folded states at equilibrium can provide detailed structural and thermodynamic information that is not accessible through kinetic experiments. This approach has been used successfully in several systems by employing protein engineering and/or the alteration of experimental conditions to stably populate intermediates.[8–12]

Comparing the equilibrium and kinetic folding reactions of structurally homologous proteins can give insight into the structural and sequence determinants of folding, including the degeneracy of the protein folding code.[13,14] A limited number of structurally related oligomeric families have been characterized, including glutathione *S*-transferases,[15,16] ketosteroid isomerases,[17–20] and histones.[21–23] This article describes the structure and stability of the isolated histone monomers H2A and H2B and examines the impact of monomer structure on folding to the native heterodimer.

The histone fold is an evolutionarily conserved DNA binding motif and forms the protein core of the eukaryotic nucleosome core particle (NCP). The histone fold has also been identified in several eukaryotic DNA binding macromolecular assemblies (e.g., several TATA-binding-protein-associated factors of the transcription factor TFIID).[24–27] The histone fold contains a long central α-helix (α2), flanked on both N- and C-termini by a β-loop and a short α-helix (α1 and α3). H2A contains a short C-terminal helix (αC) and a 20-residue unstructured C-terminal tail. H2B has a relatively long C-terminal helix (αC). The eukaryotic histone pairs, H2A–H2B and H3–H4, dimerize with a head-to-tail orientation of the two monomers, the so-called handshake motif (Fig. 1). Despite conservation of structure (backbone RMSD of ~1.5 Å),[29] the individual histone monomers have strikingly low sequence identity, between 4% and 6%. Thus, histones are an excellent model to study the degeneracy of the folding code. Several archaeal species also contain histones that function to compact DNA.[30,31] Archaeal histones are homodimeric and lack extended N- and C-terminal tails, which are the sites of regulatory posttranslational modifications in eukaryotic histones.

The folding mechanisms of archaeal and eukaryotic histones range from simple two-state processes to complex reactions with monomeric and dimeric kinetic intermediates.[21–23] There is a correlation between faster folding rates and the presence of kinetic intermediates, suggesting the hypothesis that folding through transient species is a successful method to achieve rapid folding and dimerization. The eukaryotic histone pairs, H2A–H2B and H3–H4, fold by a minimally three-state mechanism (Scheme 1): unfolded monomers rapidly form an obligatory, dimeric intermediate, $I_2$, at a rate that approaches the theoretical diffusion limit; $I_2$ then folds to the native heterodimer by a first-order process.[22,23] Because intermolecular association occurs in the dead time of the stopped-flow (SF) instrument, the presence of partially folded monomers could not be determined in previous kinetic studies. Analysis of the SF-circular dichroism (CD) burst phase in the folding of the homodimeric archaeal histone hMfB demonstrates that a partially folded monomeric ensemble is formed before dimerization.[21,32] The observation that hMfB folds ~8 times faster than the closely related hPyA1, which folds by a two-state mechanism, led to the hypothesis that monomer folding could accelerate dimerization. The transient nature and marginal stability of the hMfB monomer complicates the already inherent difficulty of studying monomers in a spontaneously homodimerizing system. However, the heterodimeric nature of the eukaryotic histones makes them ideal for studying monomers populated at equilibrium. This report represents the first thermodynamic characterization of the stability and structure of a histone monomer, an important step in understanding this biologically significant dimerization motif.

We have characterized the equilibrium structure of the isolated H2A and H2B monomers by CD and intrinsic Tyr fluorescence (FL) and determined their stability to urea-induced unfolding. Mutagenesis was used to examine the contribution of helix propensity to monomer structure and stability. The following studies indicate that partially folded H2A and H2B monomers are stabilized by helix propensity and some native-like tertiary interactions and are on-pathway for efficient heterodimer association.

## Results

### Characterization of the global structure of the H2A and H2B monomers

In the mid-1970s, the Isenberg lab pioneered the biophysical characterization of the core histones of the eukaryotic nucleosome (for review, see Ref. 33), focusing on defining the appropriate heterotypic associations found in the core nucleosome.[34] The Isenberg lab also described the dependence of the global structure and aggregation of the individual histones on pH, salt, and protein concentration. Their data suggested that the H3 and H4 histone monomers have a proclivity to homodimerize and aggregate, but self-association is minimal for isolated H2A and H2B monomers.[35,36] HPLC size-exclusion chromatography (SEC) confirmed that isolated H2A (13.9 kDa) and H2B (13.5 kDa) were monomeric under the buffer conditions and protein concentrations used in this report (Fig. 2a); the H2A–H2B dimer (27.4 kDa) is shown as a representative molecular weight standard. The slightly longer elution time of H2B relative

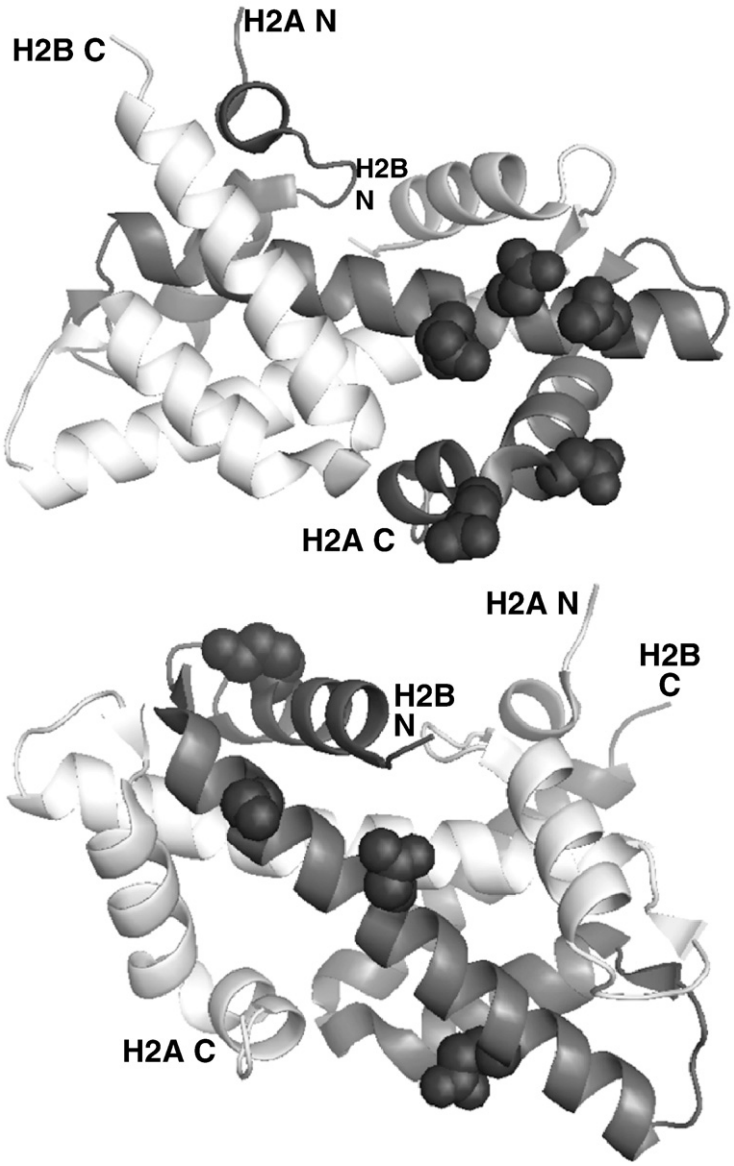


**Fig. 1.** The H2A–H2B dimer from the NCP crystal structure (Protein Data Bank code: 1kx5).[28] Residues that were mutated to Ala and Gly are shown as spheres. Upper panel: H2A is dark gray and H2B is white. Lower panel: H2A is white and H2B is dark gray. The figure was rendered using PyMOL (Delano Scientific, LLC, San Carlos, CA).

to H2A may reflect a more folded and compact structure based on spectroscopic data described below. SEC was also performed in buffers with 1 M trimethylamine-*N*-oxide (TMAO), and the monomeric elution profiles were unaltered (data not shown). No higher-order aggregates were observed in the chromatograms under these experimental conditions, with either 0 or 1 M TMAO.

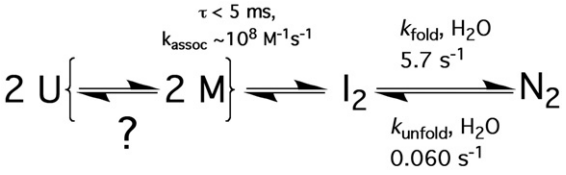


**Scheme 1.** Working mechanism for the kinetic folding of the H2A–H2B heterodimer. 2U, unfolded, dissociated H2A and H2B monomers; 2M, partially folded monomers, not directly observed by SF kinetics; $I_2$, dimeric kinetic intermediate formed in the 5-ms SF dead time, detected by SF-CD burst-phase amplitude; $N_2$, native H2A–H2B heterodimer.

The secondary structure of H2A and H2B was examined by far-UV CD (Fig. 2b). The CD spectra of each isolated monomer at 5 and 10 μM, corrected to mean residue ellipticity (MRE), were virtually identical, consistent with a lack of inappropriate homotypic associations (data not shown). Compared to the dimer, both monomers exhibit less ellipticity at 222 nm, indicative of decreased α-helical content, and greater ellipticity at 208 nm than at 222 nm, suggesting a higher random-coil content. The percentage of α-helical structure was calculated using DICROPROT, a web-based CD spectral deconvolution program that uses the Selcon2, Selcon3, and K2D algorithms.[37] The calculated helical content of H2A–H2B is 40%,[38] which is in reasonable agreement with the helical content observed in the X-ray crystal structures of the NCP, ~48%. In the absence of the heterodimeric partner, H2A and H2B are only 15% and 31% helical, respectively, as compared to ~45%

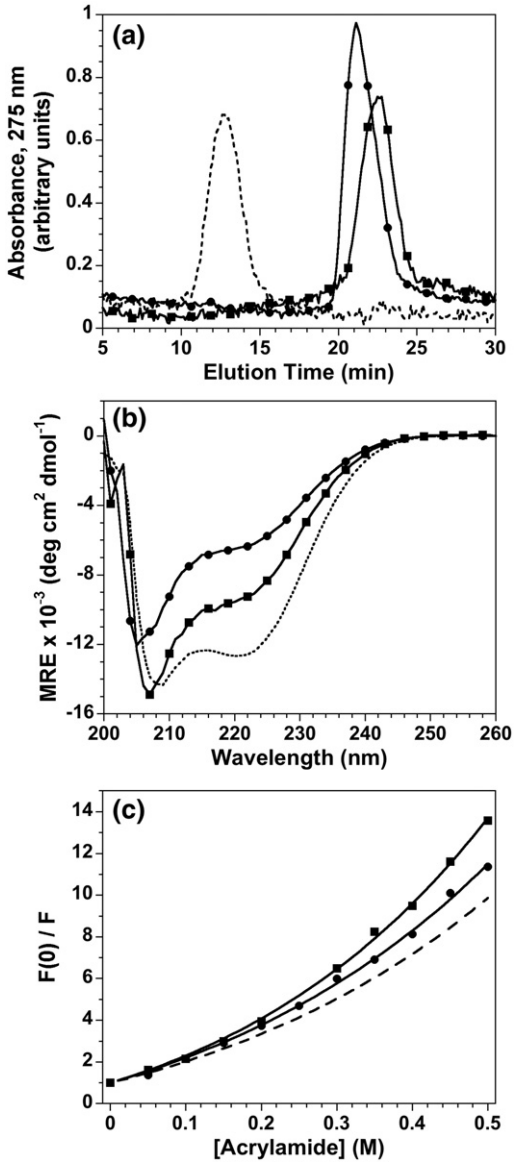


**Fig. 2.** Structural characterization of H2A and H2B monomers. In each panel, H2A is shown as circles, H2B as squares, and the H2A–H2B dimer as a broken line. (a) HPLC SEC. Histones were loaded on a BioSep-SEC-S-2000 column at 5 μM monomer and dimer. Flow rate of 0.5 ml/min. (b) Far-UV CD spectra. Protein concentrations were 5 μM monomer. (c) Acrylamide quenching of intrinsic Tyr FL at 0 M urea. Lines represent fits of the data to the Stern–Volmer equation [Eq. (1)]. Protein concentrations were 2 μM monomer. Conditions: 20 mM KPi, pH7.2, 200 mM KCl, 0.1 mM $K_2$EDTA, and ~25 °C.

for each monomer, based on the NCP crystal structure. Clearly, isolated H2B has greater helical content than H2A, which is in contrast to the sequence-based predictions of AGADIR.[39] Overall, AGADIR predicts helical content of only 1–4% for the histone monomers, and the predicted content of H2A is consistently higher than that of H2B over a range of condition parameters (ionic strength and temperature).

The tertiary structure in the monomers was examined by intrinsic Tyr FL. H2A contains three Tyr residues located in the first β-loop and α2; these residues are largely solvent inaccessible in the native dimer, with the majority of the burial resulting from intermonomer contacts. H2B has five Tyr residues spread throughout the primary structure. Three Tyr residues are at the N-terminus of α1; two are highly buried in the native dimer, but all make significant intramonomer contacts. Tyr80 at the C-termini of α2 is largely solvent exposed in the native state. The fifth Tyr is in αC and is highly buried in the dimer interface. The relative solvent accessibility of the Tyr residues was examined by acrylamide quenching of FL in the native and unfolded monomers. Stern–Volmer plots for the folded monomers and the H2A–H2B dimer are shown in Fig. 2c. The nonlinear dependence on the quencher concentration indicates quenching by both dynamic and static mechanisms. The values for the dynamic and static quenching constants, $K_{SV}$ and $V$, respectively, are given in Table 1. Unfolding has minor effects on static quenching with changes of 0.9- to 1.2-fold for the $V$ value. However, upon unfolding, dynamic quenching increases by 1.3- and 1.5-fold for the H2A and H2B monomers, respectively. An even larger change, 1.7-fold, is observed upon unfolding of the H2A–H2B dimer. These data demonstrate that the Tyr residues are excluded from solvent in the folded monomers but to a significantly lower extent than in the folded dimer. Similar results were observed in the presence of 1 M TMAO (data not shown).

## Equilibrium stability of the H2A and H2B monomers

The stability of the histone monomers was determined by urea-induced equilibrium titrations, monitored by far-UV CD and Tyr FL. Unfolding transitions must have well-defined native and unfolded baselines to extract reliable thermodynamic parameters using Eq. (2). In the standard buffers used to determine the stability of the H2A–H2B dimer,[40] the isolated monomers are only marginally stable, and the equilibrium transitions lacked well-defined native baselines (Fig. 3a). The osmolyte TMAO stabilizes proteins and extends the native baseline in equilibrium titrations.[41–43] TMAO has been used previously to stabilize histone oligomers.[21,44,45] The

**Table 1.** Stern–Volmer constants for acrylamide FL quenching

| Histone | [Urea] (M) | $K_{SV}$ ($M^{-1}$) | $V$ ($M^{-1}$) |
|---|---|---|---|
| H2A | 0 | 9.11 (0.54) | 1.45 (0.11) |
| H2B | 0 | 9.41 (0.57) | 1.75 (0.11) |
| H2A–H2B | 0 | 7.49 (0.46) | 1.47 (0.11) |
| H2A | 5 | 13.31 (0.53) | 1.32 (0.09) |
| H2B | 5 | 12.03 (0.33) | 1.96 (0.06) |
| H2A–H2B | 5 | 12.78 (0.62) | 1.75 (0.09) |

Conditions: 2 μM monomer, 200 mM KCl, 20 mM KPi, pH 7.2, 0.1 mM $K_2$EDTA, and 25 °C. The standard deviation of the fits is given in parentheses. The Stern–Volmer constants, $K_{SV}$ and $V$, describe dynamic and static quenching, respectively.

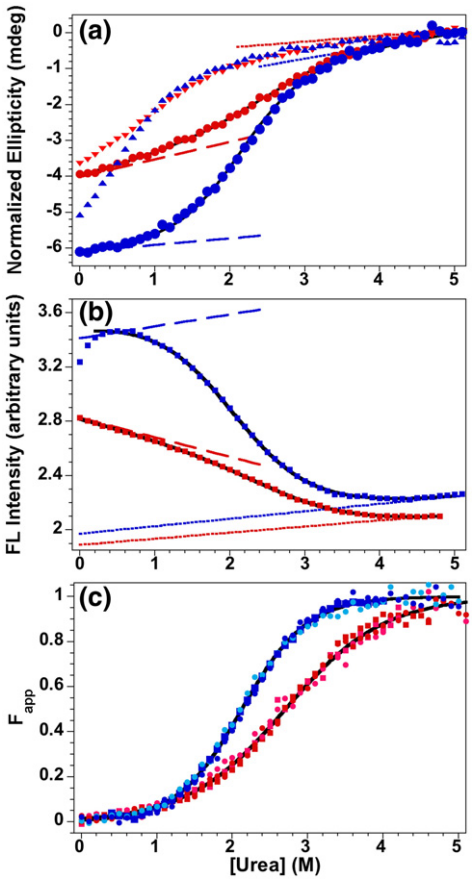


**Fig. 3.** Representative urea-induced equilibrium unfolding transitions for WT monomers. For all panels: H2A data, red; H2B data, blue; continuous lines represent global fits to a two-state monomeric unfolding model; folded and unfolded baselines are indicated by broken and dotted lines, respectively. (a) Far-UV CD data at 222 nm at 10 μM monomer in 1 M TMAO (circles, with fitted lines) and 0 M TMAO (triangles). (b) FL data at 308 nm at 10 μM monomer. (c) $F_{app}$ curves for H2A and H2B at 5 and 10 μM (light and dark shades, respectively) for CD (circles) and FL (squares). Conditions: 1 M TMAO (except where noted), 200 mM KCl, 20 mM KPi, pH7.2, 0.1 mM $K_2$EDTA, and 25 °C.

H2A and H2B monomers were sufficiently stabilized by 1 M TMAO to allow determination of native baselines (Fig. 3). As noted above, 1 M TMAO did not induce homotypic interactions in either H2A or H2B. The secondary-structure content of H2B is enhanced by TMAO, but only modest effects are seen for H2A (Fig. 3a).

For each histone monomer, data sets of five to six titrations were used for local and global fitting to a two-state monomer unfolding model. The data sets included titrations initiated from the folded and unfolded state and titrations at both 5 and 10 μM monomer. Unfolding and refolding titrations were coincident (data not shown), demonstrating a highly reversible equilibrium process without hysteresis. The local fits of the CD and FL titrations were in good agreement and exhibited no protein concentration dependence (Fig. 3c). This agreement demonstrates that unfolding is a unimolecular, two-state process, with no detectable equilibrium intermediates. The entire data set for each monomer was then globally fit, with linked $\Delta G°(H_2O)$ and $m$ values. The global fits are shown as the lines in Fig. 3, and the fitted parameters are given in Table 2. The globally fitted parameters are in excellent agreement with the average values from the local fits (data not shown).

The H2A and H2B monomers are much less stable than the H2A–H2B dimer (15.5 kcal $mol^{-1}$ in 1 M TMAO at a standard state of 1 M dimer[45]), demonstrating that dimerization contributes significantly to the overall stability of the native dimer. The lower $\Delta G°(H_2O)$ and $m$ values of H2A relative to H2B demonstrate that the H2A monomer is less stable and buries less surface area, consistent with H2A's diminished ellipticity at 222 nm (Fig. 2b) and shorter elution time in HPLC SEC (Fig. 2a).

## Kinetic folding of H2A–H2B from partially folded monomers

To determine if the folded, isolated monomers are an appropriate equilibrium model for potential kinetic intermediates, we performed SF kinetic refolding experiments. The working mechanism of H2A–H2B folding (Scheme 1) predicts rapid monomer folding prior to dimerization. As expected, the refolding of the individual monomers from 4 M urea is complete in the SF dead time (data not shown). In previous kinetic studies, refolding of H2A–H2B was initiated from unfolded dimer; that is, a pool of both monomers unfolded in 4 M urea.[23] In the current study, folding was initiated by mixing folded H2A and H2B monomers from different syringes. SF-FL and SF-CD data were collected at final monomer concentrations of 7.5, 15, and 30 μM. As observed previously for refolding from 4 M urea,[23] there was a significant SF-CD burst phase, and the observed CD and FL kinetic responses were well fit by a single, first-order exponential function. The rates were largely independent of protein concentration, varying only 1.3-fold over a 4-fold range of monomer concentrations. This is consistent with the published mechanism (Scheme 1), in which dimerization occurs in the 5-ms SF dead time, and the observed kinetic phase is the conversion of a dimeric kinetic intermediate ($I_2$) to the native dimer ($N_2$).

Kinetic responses were compared for folding to a final urea concentration of 0.4 M and 7.5 μM monomer from three initial conditions. Monomers were pre-equilibrated separately in 0 or 0.4 M urea and then mixed to initiate refolding; the kinetic responses fit to rates of 2.5±0.2 $s^{-1}$ and 2.6±0.5 $s^{-1}$, respectively. Previous refolding studies from unfolded monomers in 4 M urea gave a globally fitted rate of 2.7 $s^{-1}$.[23] The excellent agreement of these rates, despite different initial conditions (favoring unfolded or folded monomers), indicates that the monomeric structures populated at low urea concentrations are consistent with an on-pathway kinetic intermediate species. Preliminary data show that the urea dependence of the rates is also similar for re-

**Table 2.** Parameters describing the equilibrium stability of the WT and mutant histones

| | | Monomer parameters (1 M TMAO) | | | Dimer parameters | | |
|---|---|---|---|---|---|---|---|
| | | $\Delta G°(H_2O)$ (kcal $mol^{-1}$) | *m* value (kcal $mol^{-1}$ $M^{-1}$) | $\Delta C_M$[a] (M urea) | $\Delta G°(H_2O)$ (kcal $mol^{-1}$) | *m* value (kcal $mol^{-1}$ $M^{-1}$) | $\Delta C_M$[a]b (M urea) |
| *H2A* | | | | | | | |
| WT | | 2.45 (0.06) | 0.91 (0.04) | [2.69] | 11.8 | 2.9 | [1.72] |
| E61A | α2 | 2.93 (0.12) | 0.87 (0.07) | −0.68 | 11.6 (0.1) | 2.8 (0.1) | 0.00 |
| E61G | | 2.04 (0.08) | 0.89 (0.06) | 0.40 | 10.3 (0.1) | 2.9 (0.1) | 0.49 |
| E64A | α2 | 2.93 (0.09)[b] | 1.08 (0.11)[b] | ca. −1.5 | 12.3 (0.2) | 2.7 (0.1) | −0.32 |
| E64G | | 2.57 (0.12) | 0.90 (0.07) | −0.16 | 11.2 (0.1) | 2.9 (0.2) | 0.23 |
| N68A | α2 | 3.34 (0.47) | 1.40 (0.20) | 0.23 | 10.9 (0.2) | 2.7 (0.1) | 0.25 |
| N68G | | 2.42 (0.14) | 0.92 (0.09) | 0.06 | 10.0 (0.1) | 2.8 (0.1) | 0.56 |
| N89A | α3 | 2.91 (0.25) | 1.09 (0.16) | 0.02 | 11.2 (0.1) | 2.9 (0.1) | 0.19 |
| N89G | | 2.52 (0.25) | 1.00 (0.09) | 0.19 | 11.4 (0.1) | 2.9 (0.1) | 0.15 |
| E91A | αC | 2.60 (0.31) | 0.97 (0.10) | 0.01 | 11.4 (0.2) | 2.8 (0.1) | 0.05 |
| E91G | | 2.11 (0.08) | 0.97 (0.04) | 0.51 | 11.0 (0.1) | 2.9 (0.1) | 0.26 |
| *H2B* | | | | | | | |
| WT | | 2.90 (0.07) | 1.37 (0.05) | [2.12] | 11.8 | 2.9 | [1.72] |
| K43A | α1 | 3.48 (0.22) | 1.27 (0.12) | −0.42 | 10.9 (0.1) | 2.6 (0.1) | 0.12 |
| K43G | | 2.92 (0.12) | 1.41 (0.09) | 0.05 | 10.9 (0.1) | 2.8 (0.1) | 0.27 |
| S57A | α2 | 2.98 (0.12) | 1.44 (0.09) | 0.05 | 11.4 (0.1) | 2.6 (0.1) | −0.04 |
| S57G | | 2.54 (0.04) | 1.37 (0.04) | 0.30 | 11.0 (0.1) | 2.8 (0.1) | 0.22 |
| N64A | α2 | 3.05 (0.17) | 1.38 (0.10) | −0.09 | 11.2 (0.1) | 2.8 (0.1) | 0.18 |
| N64G | | 2.55 (0.25) | 1.08 (0.14) | −0.24 | 10.0 (0.1) | 2.9 (0.1) | 0.62 |
| E73A | α2 | 2.43 (0.05) | 1.38 (0.04) | 0.36 | 11.3 (0.1) | 2.9 (0.1) | 0.14 |
| E73G | | 2.34 (0.09) | 1.45 (0.08) | 0.51 | 10.3 (0.1) | 2.9 (0.1) | 0.50 |

Conditions: 200 mM KCl, 20 mM KPi, pH7.2, 0.1 mM $K_2$EDTA, and 25 °C. The $\Delta G°(H_2O)$ and *m* values were determined global fits of multiple CD and FL titrations at varied protein concentrations. Values in parentheses represent the uncertainty at one standard deviation from the rigorous error analysis.[46] The WT dimer values were published previously.[38]

[a] $C_M$ is [Urea] at which unfolded monomers constitute 50% of the population. The WT values are given in brackets. $\Delta C_M = \Delta C_{M,\ WT} - \Delta C_{M,\ mutant}$; a negative value indicates a higher $C_M$ for the mutant. The $C_M$ values for a dimer are protein concentration dependent; the dimer $\Delta C_M$ values were calculated for 10 μM monomer.

[b] The H2A E64A mutation was not completely unfolded at 5 M urea in 1 M TMAO. Therefore, the $\Delta G°(H_2O)$ and *m* values were determined at 0 M TMAO. The $C_M$ value in 1 M TMAO was estimated to be ~4.2 M urea; this value was used in calculating the $\Delta C_M$ given in the table.

folding from folded and unfolded monomers (M.R.S. and L.M.G., unpublished results).

## Mutations to evaluate contributions of helical propensity in the H2A and H2B monomers

To further elucidate regions of secondary structure and stability within the partially folded H2A and H2B monomers, we introduced a series of Ala and Gly mutations into the histone monomers. Three criteria were used to select the mutation sites. First, to minimize disruption of side-chain packing, we targeted only highly solvent-exposed residues (Fig. 1). Second, a majority of the variants were created in the α2 helix of the histone fold. Previous experiments suggest that this helix contributes to the structure of the monomeric kinetic intermediate and the dimerization transition state of the archaeal histones hMfB and hPyA1.[32] Residues in the N-terminus of H2A α2 were not mutated because this region is largely buried in the H2A–H2B dimer by the noncanonical αC helix of H2B. Third, AGADIR, a helix-content prediction algorithm,[39] was used to guide selection toward regions predicted to have higher helicity. The mutations are listed in Table 2 and are shown in Fig. 1. Each of the nine selected residues was mutated to both Ala and Gly to tease apart effects from side-chain truncation and altering helix propensity. It is known that mutations can affect the stability of the folded or unfolded state; attributing effects to the unfolded ensemble is difficult without kinetic data or additional orthogonal perturbations. However, examination of the three-dimensional structure of the H2A–H2B dimer allows the suggestion of plausible effects on the native state, which are highlighted in the discussion of the mutants.

H2A residues: AGADIR predicts minimal helicity in α1, the first two turns of the central α2 helix, and the α3 helix of the histone fold. Significant helicity is predicted for residues 52 to 67 of α2 as well as the short αC helix. Glu61, Glu64, and Asn68 are in the C-terminal half of the central helix. Asn89 is a C-terminal cap of α3, and Glu91 is in the first turn of αC.

H2B residues: The predictions of AGADIR suggest significant helicity in α1 and only moderate helical content in the C-terminal half of α2 and all of α3. Lys43 is in α1, and Ser57, Asn64, and Glu73 are in the N-terminal, middle, and C-terminal regions of α2.

## Far-UV CD and stability of the H2A and H2B monomer mutants

The far-UV CD spectra of the mutants were analyzed with DICROPROT.[37] Representative CD spectra of Ala and Gly mutants of H2A Glu64 and H2B Glu73 are shown in Fig. 4a and c. With the exception of N89A (a helix-capping residue), the H2A Ala mutations increased helical content by 1.3- to 1.6-fold.

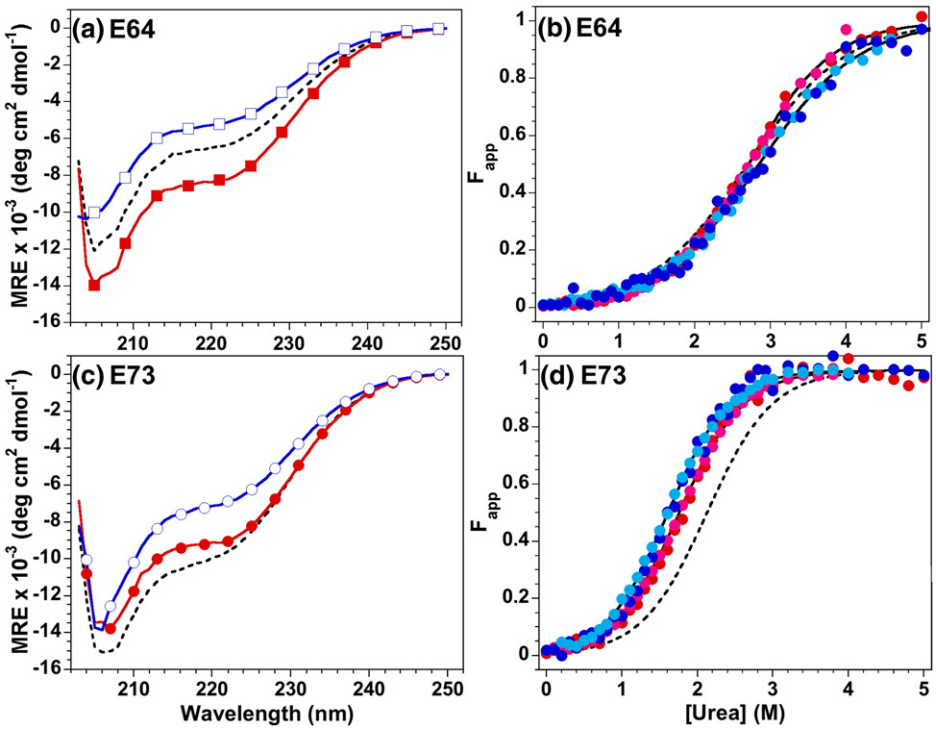


**Fig. 4.** Representative data showing the effects of the helix propensity variants on monomer structure and stability. (a) Far-UV CD spectra and (b) $F_{app}$ curves of H2A E64A (red, in 0 M TMAO) and E64G (blue, in 1 M TMAO). (c) Far-UV CD spectra and (d) $F_{app}$ curves of H2B E73A (red) and E73G (blue). $F_{app}$ curves were determined from equilibrium unfolding titrations monitored by far-UV CD at 222 nm (dark shades) and Tyr FL at 308 nm (light shades), and the continuous lines represent global fits of the data sets to a two-state monomeric unfolding model. In all panels, the WT histone data are represented by a broken line. Superimposable data were collected at 5 and 10 μM monomer, but for clarity, only the 5-μM data are shown. Conditions are given in the legend to Fig. 3; the CD spectra were determined in 0 M TMAO; the equilibrium urea titrations were performed in 1 M TMAO, except for H2A E64A.

The helical content of E64G and N68G decreased by 1.4- and 1.2-fold, while E61G and E91G had little effect. The 13% decrease in helicity observed for both N89A and N89G points to the importance of the helix-capping interactions of the Asn side chain in promoting helix structure. The H2B Ala mutations uniformly diminish helicity by 10–15%, suggesting the importance of side-chain interactions in stabilizing helical structure. The Gly substitutions have more pronounced effects, decreasing helical content by 1.4- to 1.7-fold.

The stabilities of the H2A and H2B variants were determined in 1 M TMAO as described above for the WT monomers. The parameters describing the equilibrium unfolding are given in Table 2, and representative titrations are shown in Fig. 4b and d. The $F_{app}$ (apparent fraction of unfolded monomer) curves for all other histone mutants are shown in Supplementary Figs. S1 and S2. Stability effects are reported as $\Delta C_M$ (the difference in the midpoint of the unfolding transition) in Table 2 and $\Delta\Delta G°(H_2O)$ in Table 3. With the exception of H2A N68A and H2B N64G, the *m* values are within 10% of the WT values. However, even small *m* value changes can result in lower $C_M$ values (positive values in Table 2) despite stabilizing (negative) $\Delta\Delta G°(H_2O)$ values.

H2A Ala mutations at Asn89 and Glu91 have minimal effects on stability, while E61A, E64A, and N68A are significantly stabilizing. E64A was stabilized to the extent that, in 1 M TMAO, complete unfolding (and determination of an unfolded baseline) could not be achieved within the limits of urea solubility. Therefore, the equilibrium parameters for E64A in Table 2 were determined in 0 M TMAO, making it difficult to compare accurately to the other H2A variants. Of the H2A Gly mutants, only E61G and E91G were significantly destabilizing. These results are consistent with WT H2A having minimal secondary structure and stability (Figs. 2b and 3), such that Gly substitutions do not dramatically destabilize existing structure, but the increased helix propensity of Ala can induce folding.

In α1 of H2B, K43A was strongly stabilizing, while K43G had no effect. Ala substitutions in the N-terminal and central portion of α2 (S57A and N64A) had minimal effects, but E73A toward the C-terminus was destabilizing. The comparable Gly substitutions (S57G, N64G, and E73G) were all destabilizing, by 0.3 to 0.6 kcal $mol^{-1}$. The similar destabilization by E73A and E73G suggests that an electrostatic interaction between Glu73 and Arg76 contributes more to stability than helix propensity.

Comparison of the free energies of unfolding for the Ala and Gly mutations, $\Delta\Delta G°$(Ala–Gly), minimizes effects from side-chain interactions and allows a more direct assessment of the impact of helix propensity. Only H2B Glu73, near the end of α2, did not exhibit a significant $\Delta\Delta G°$(Ala–Gly). The largest

**Table 3.** Comparison of mutational effects on the histone monomers and dimers

| | | ΔΔG for the monomer mutations[a] (kcal mol$^{-1}$) | | | ϕ-Value comparison to effects on dimer stability[b] | |
|---|---|---|---|---|---|---|
| | | Gly | Ala | Ala–Gly | ϕ Gly | ϕ Ala–Gly |
| *H2A* | | | | | | |
| Glu61 | α2 | 0.4 | −0.5 | 0.9 | 0.3 | 0.7 |
| Glu64[c] | α2 | −0.1 | −1.3 | 1.2 | ~0 | 1.2 |
| Asn68 | α2 | 0.0 | −0.9 | 0.9 | ~0 | 1.1 |
| Asn89 | α3 | 0.0 | −0.5 | 0.4 | ~0 | –[d] |
| Glu91 | αC | 0.3 | −0.2 | 0.5 | 0.4 | 1.0 |
| *H2B* | | | | | | |
| Lys43 | α1 | 0.0 | −0.6 | 0.6 | 0.0 | –[d] |
| Ser57 | α2 | 0.4 | −0.1 | 0.5 | 0.5 | 1.2 |
| Asn64 | α2 | 0.4 | −0.2 | 0.5 | 0.2 | 0.4 |
| Glu73 | α2 | 0.6 | 0.5 | 0.1 | 0.4 | 0.1 |

Calculations are derived from data presented in Table 2.

[a] The column heading indicates the ΔΔ*G* convention. For example, $\Delta\Delta G_{Gly} = \Delta G°(H_2O)_{WT} - \Delta G°(H_2O)_{Gly\ mutant}$ or $\Delta\Delta G_{Ala-Gly} = \Delta G°(H_2O)_{Ala\ mutant} - \Delta G°(H_2O)_{Gly\ mutant}$. Positive values indicate that the mutation is destabilizing or that Ala affords greater stability than Gly at that position.

[b] ϕ values represent the ratio of the ΔΔ*G* values for the monomer and dimer. ϕ Gly = $(\Delta\Delta G_{Gly\ monomer})/(\Delta\Delta G_{Gly\ dimer})$. ϕ Ala–Gly = $(\Delta\Delta G_{Ala-Gly,monomer})/(\Delta\Delta G_{Ala-Gly,dimer})$.

[c] The $\Delta G°(H_2O)$ in 1 M TMAO for H2A E64A monomer was estimated from the relationship $\Delta G°(H_2O) = C_M \times m$, with an estimated $C_M$ of 4.2 M (see Table 2 legend) and assuming the WT *m* value of 0.9 kcal mol$^{-1}$; a higher $\Delta G°(H_2O)$ value is estimated if the E64A *m* value in 0 M TMAO is used.

[d] No ϕ value is given because the ΔΔ*G*°(Ala–Gly) for the heterodimer was very small.

helix propensity effects were at the C-terminal half of α2 in H2A, with ΔΔ*G*°(Ala–Gly) values of ≥0.9 kcal mol$^{-1}$. Other H2A and H2B mutational pairs exhibited more moderate helix propensity effects, with ΔΔ*G*°(Ala–Gly) values of 0.4 to 0.6 kcal mol$^{-1}$.

## Far-UV CD and stability of the H2A–H2B dimer mutants

To assess whether the effects of mutations on monomer stability were from native or nonnative interactions, we determined the far-UV CD spectra and the equilibrium stability of the mutant heterodimers. Representative CD spectra are shown in Fig. 5a for H2A-Glu64 and H2B-Glu73 mutants. All mutant dimers exhibited CD spectra with similar shape and minima at 208 and 222 nm. The DICROPROT deconvolution program[37] predicted helical content within 5–10% of WT for most mutants. Both H2B K43A and K43G exhibited ~20% less helicity than WT, suggesting that disruption of an electrostatic interaction in the folded dimer influences structure more than helix propensity. Gly substitutions at H2A-Glu64, H2B-Ser57, and H2B-Glu73 had 1.3-fold less helicity than the WT dimer.

Urea-induced equilibrium titrations were performed to determine the stability of the mutant heterodimers. Five to six titrations were collected for each dimer at multiple dimer concentrations between 2 and 10 μM dimer. Local fits of individual titrations demonstrated that the transitions were protein concentration dependent and that transitions monitored by CD and FL were superimposable; this

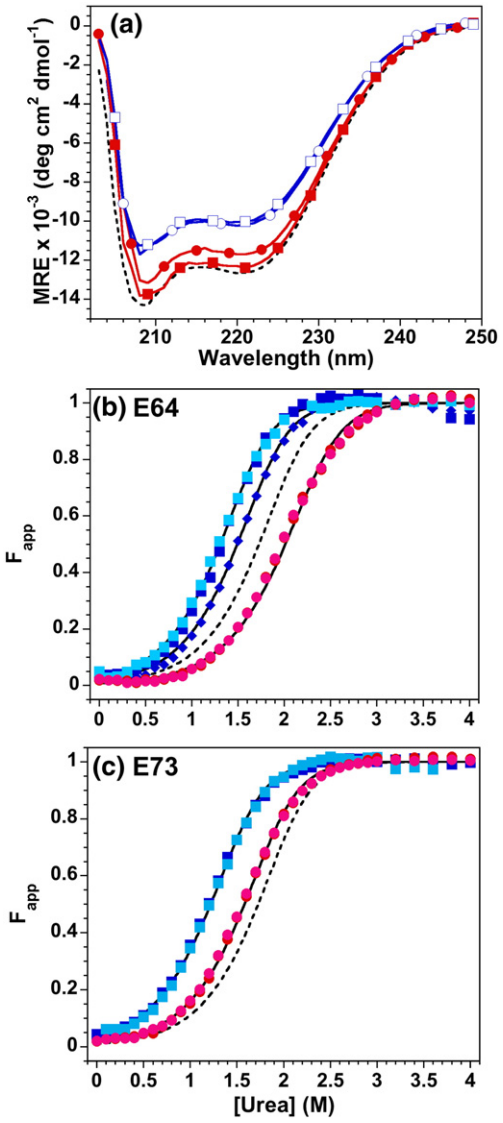


**Fig. 5.** Representative data showing the effects of the helix propensity mutations on the H2A–H2B dimer. (a) Far-UV CD spectra, normalized to mean residue ellipticity, for WT H2A–H2B (black broken line), H2A-E64A/G (squares), and H2B E73A/G (circles); spectra for the Ala and Gly mutants are identified by red filled and blue open symbols, respectively. (b and c) Representative $F_{app}$ curves for far-UV data at 222 nm (dark shades) and Tyr FL data at 308 nm (light shades). Continuous lines represent global fits of the data sets to a two-state dimeric unfolding mechanism; for comparison, the equilibrium transition of the WT heterodimer is shown (broken line).[40] Unfolding data were collected up to 5 M urea but are not shown to allow expansion of the transition region. (b) H2A E64A (red circles) and E64G (blue squares) at 2 μM monomer; data for E64G at 5 μM monomer (blue diamonds) are shown as an example of the protein concentration dependence of the dimeric unfolding transition. (c) H2B N64A (red circles) and N64G (blue squares) at 2 μM monomer. Buffer conditions: 200 mM KCl, 20 mM KPi, pH7.2, 0.1 mM $K_2$EDTA, and 25 °C.

result is consistent with a two-state equilibrium unfolding reaction and no detectable equilibrium intermediates. As described previously for WT H2A–H2B,[40] the data sets for the heterodimer variants were fit globally by a dimeric, two-state equilibrium model. The $\Delta G°(H_2O)$ and $m$ values were treated as global parameters and linked across all titrations for a given dimer. The fitted parameters are given in Table 2. Representative $F_{app}$ plots for the Ala and Gly variants of H2A Glu64 and H2B Glu73 are shown in Fig. 5b and c; the global fits are shown as continuous lines through the data points. $F_{app}$ curves for all other heterodimer mutants are shown in Supplementary Figs. S3 and S4.

H2A variants: The only stabilizing mutation was E64A. While destabilizing, the other four H2A Ala mutations exhibited stabilities within 10% of WT. Except for the C-terminal helix cap residue Asn89, mutations to Gly were significantly more destabilizing than the Ala mutations, yielding $\Delta\Delta G°$(Ala–Gly) values of 0.5 to 1.3 kcal $mol^{-1}$.

H2B variants: All mutations were destabilizing, with Gly being more destabilizing than Ala, particularly by comparison of $C_M$ values. Replacement of Lys43 by Ala and Gly resulted in $\Delta G°(H_2O)$ values that were 0.9 kcal $mol^{-1}$ lower than WT, suggesting that the loss of the Lys43–Asp48 salt bridge is the major contributor of this residue to the stability of the dimer. In contrast, the $\Delta\Delta G°$(Ala–Gly) for mutations at Ser57, Asn64, and Glu73 ranges from 0.4 to 1.2 kcal $mol^{-1}$.

As observed for monomer stability, the H2A and H2B mutations demonstrate that the α2 helix is the most sensitive to changes in helix propensity, as indicated by larger $\Delta\Delta G°$(Ala–Gly) values. In contrast to the monomers, where the Ala mutations are slightly to significantly stabilizing (except H2B-E73A), most Ala mutations in the heterodimer result in measurable destabilization of the heterodimer. This difference in the effects of the mutations on the stabilities of the monomers and the heterodimer highlights the role of nonnative interactions in the partially folded structure of the isolated monomers.

## Discussion

### Structural and thermodynamic characterization of the WT H2A and H2B monomers

Deconvolution of far-UV CD spectra (Fig. 2b) suggests that ~20 of the 129 residues of H2A and ~38 of the 122 residues of H2B are in a helical conformation, as compared to ~100 residues in the H2A–H2B dimer.[38] Thus, folding in the individual monomers may comprise ~60% of the helical structure formed in the native dimer. Acrylamide quenching of Tyr FL shows that the monomers also contain some tertiary structure that excludes Tyr residues from solvent (Table 1 and Fig. 2c). However, the H2A and H2B monomers are quite unstable compared to typical globular monomeric polypeptides of similar size. At a 1-M standard state (in 1 M TMAO), the $\Delta G°(H_2O)$ values of H2A and H2B are significantly less than that of the H2A–H2B dimer. A more informative comparison is at the protein concentration of the experimental conditions, for example, 10 μM monomer, rather than 1 M monomer compared to 1 M dimer. The stability of the isolated monomers is protein concentration independent, but the $\Delta G(H_2O)$ value of the H2A–H2B dimer at 10 μM monomer is 8.7 kcal $mol^{-1}$. By this comparison, the $\Delta G(H_2O)$ values of the isolated monomers are ~30% that of the native dimer. To the extent that monomer stability arises from native interactions, the $\Delta G$ of the dimer can be approximated by $\Delta G_{dimer} = (\Delta G_{H2A} + \Delta G_{H2B} + \Delta G_{dimerization})$. Thus, at 10 μM monomer, the stability achieved by monomer folding may constitute ~60% of the stability of the heterodimer.

The $m$ value describes the steepness of the unfolding transition; in a two-state system, this parameter is protein concentration independent and correlates with the change in solvent accessible surface area between the unfolded and native states, ΔASA.[47] The $m$ value for H2A–H2B can be parsed into three components as described for $\Delta G_{dimer}$. The sum of the monomer $m$ values, 2.3 kcal $mol^{-1}$ $M^{-1}$, is 85% of that determined for the native dimer in 1 M TMAO, 2.7 kcal $mol^{-1}$, suggesting that substantial surface area is buried by monomer folding. Expected ΔASA and $m$ values were calculated by the method of Meyers *et al.*[47] using the structure of the H2A–H2B dimer in the NCP.[29] The calculated ΔASA for the native dimer unfolding to two unfolded monomers (i.e., $N_2$ to 2U) is ~16,800 $Å^2$, corresponding to a predicted $m$ value of ~2.8 kcal $mol^{-1}$ $M^{-1}$,[40] in excellent agreement with experimental $m$ values in 0 and 1 M TMAO.

The ΔASA for dimer dissociation to two fully folded monomers, assuming no unfolding upon dissociation, was calculated using the coordinates for the individual H2A and H2B chains from the structure of the H2A–H2B dimer in the NCP. This calculation gives the minimal ΔASA value of ~5200 $Å^2$.[44] A noteworthy feature of this calculated ΔASA is that the vast majority of surface area exposed in this *in silico* dissociation is from folded helices and β-loops in the H2A–H2B dimer interface. Since these regions are fully folded and compact in the X-ray structure determined in the absence of TMAO, it is unlikely that this stabilizing osmolyte would significantly alter this estimate of the minimal ΔASA between 2M and $N_2$. Using the Myers *et al.* formula,[47] the ΔASA of 5200 $Å^2$ predicts a minimal $m$ value of ~0.9 kcal $mol^{-1}$ $M^{-1}$ for the folding of 2M to $N_2$. Thus, the $m$ value associated with monomer folding (2U to 2M) should be ~67% of the experimentally determined $m$ value for 2U to $N_2$; this estimate reflects an upper limit because of the assumption that no unfolding occurs upon dissociation, which is unlikely because the CD spectra show that the isolated monomers have significantly less secondary structure than the monomers in the context of the native dimer.

In conclusion, the difference between ΔASA values predicted for the monomers from experimental

$m$ values (ΔASA ~85% of $N_2$) and that predicted from structure (ΔASA <67% of $N_2$) indicates that isolated monomers are overly collapsed, with greater solvent exclusion than in the extended handshake motif. One concern of this interpretation is that a stabilizing osmolyte such as TMAO might induce this overly collapsed structure. If this were the case, lower $m$ values (and lower ΔASA values) would be expected in the absence of TMAO. Without well-defined native baselines, accurate $m$ values could not be determined in 0 M TMAO for the WT monomers. However, the slopes of the transitions in the CD titrations in 0 and 1 M TMAO are nearly parallel (H2A and H2B, Fig. 3a). Similar parallel transitions at 0 and 1 M TMAO are observed for the much stabilized H2A-E64A mutant (data not shown). These comparisons strongly suggest that the $m$ values, and thus the ΔASA, of the H2A and H2B monomers are fairly independent of TMAO, as reported previously for other monomeric proteins.[48]

### Equilibrium monomeric H2A and H2B as models for kinetic folding intermediates

SF kinetics cannot directly address monomer association because dimerization occurs in the burst phase at the lowest feasible monomer concentration accessible by far-UV CD or Tyr FL. However, the kinetic data do probe the similarity of the $I_2$ ensembles formed from partially folded and unfolded monomers. If the structure in the isolated monomers is unproductive and a kinetic trap, then significantly slower rates should be observed relative to refolding from urea-denatured monomers. However, similar kinetics were observed for folding from isolated, partially folded monomers and urea-unfolded monomers. This result demonstrates that folding in the monomers is not a significant impediment to rapid, efficient folding. Furthermore, the data suggest that the partially folded monomers studied here at equilibrium are similar to putative kinetic monomeric intermediates indicated by the question mark in Scheme 1.

### Contribution of residues to the stability of H2A and H2B monomers

A series of 18 mutants were characterized to determine regions that are structured in the histone monomers. These mutational studies address two questions: Does the residue contribute to the stability of the isolated histone monomer? To what extent does helix propensity at that site contribute to stability? Interpreting the effects of Ala mutations can be complicated; side-chain truncation can be destabilizing by eliminating stabilizing tertiary interactions but may be offset by a stabilizing increase in helix propensity. However, if mutation of a residue to Gly (side-chain truncation and decreased helix propensity) causes minimal changes in stability, the residue presumably does not contribute to the structure and stability of the monomer. The magnitude of the $\Delta\Delta G°$(Ala–Gly) reflects the relative importance of helix propensity of the mutated residue to the stability of the monomer. There is a significant correlation between the monomer $\Delta\Delta G°$(Ala–Gly) values and changes in helicity determined by far-UV CD; the only exception is H2B Glu73, which is the only Ala substitution that destabilizes the isolated monomers. No correlation is observed for the effects on the dimer. These two results suggest that helix propensity and secondary structure are predominant contributors to monomer stability, while tertiary or quaternary structures and side-chain interactions are more important in dimer stability and stabilizing the helical structures observed in the dimer.

Comparison of a mutation's effects on the stability of the monomer and the heterodimer provides insights into how "folded" the residue is in the monomer—akin to the popular ϕ-value analyses to monitor the contribution of residues to transition state structure—and whether the interaction is native or nonnative. ϕ-Value analyses do not necessarily assume that the effect of mutations is on the native state; the analyses are valid whether the mutations stabilize the unfolded ensemble or destabilize the native state.[49] In Table 3, the $\Delta\Delta G°$ values are provided for the monomer mutants, as well as the ϕ values for the effects of Gly substitutions and comparison of the $\Delta\Delta G°$(Ala–Gly) values for monomer and dimer stability. The ϕ Ala–Gly parameter has three advantages. First, the reliability of using small perturbations in stability for calculation of ϕ values (i.e., dividing by small $\Delta\Delta G$ values) has been criticized recently in the literature.[50,51] The monomer and dimer $\Delta\Delta G°$(Ala–Gly) values are generally similar or larger than the $\Delta\Delta G°$(Ala) values. Second, as noted above, Ala substitutions can have offsetting effects of enhancing helix propensity while abrogating favorable tertiary interactions. A standardized change in helix propensity across all nine sites can be obtained by comparing the effects of Ala and Gly mutations at a given position, with minimal differences in potential side-chain interactions. Third, the Ala–Gly comparison circumvents the complication that most of the Ala monomer mutations are stabilizing and exhibit negative $\Delta\Delta G°$ values.

These analyses have the caveat that the $\Delta\Delta G°$ values for the mutant monomers were determined in 1 M TMAO, while the values for the heterodimer mutants were measured in the absence of TMAO. However, there is a well-established linear dependence of $\Delta G°(H_2O)$ on TMAO concentration,[41–43] which has also been observed for the WT H2A–H2B dimer (P. J. Guyett and L. M. Gloss, unpublished results). If the slope of this linear dependence, the TMAO $m$ value, is not affected by mutation, then the $\Delta\Delta G°$ values for the mutant heterodimer should be largely independent of TMAO concentration. Firstly, this lack of effect for mutation of side chains is reasonable to expect because the solvophobic stabilization by TMAO is predominantly through modulating the interactions of solvent with the peptide

backbone.[52,53] Secondly, this lack of effect has been observed for an unrelated set of H2A–H2B mutations (P. J. Guyett and L. M. Gloss, unpublished results) and other proteins.[48,54] Thirdly, the current understanding is that denaturants (urea) and osmolytes (TMAO) are simply different ends of a spectrum and act independently, with a linear dependence on their concentration, to modulate a protein's equilibrium stability.[48,53] Accordingly, the urea *m* value of WT H2A–H2B does not change significantly between 0 and 1 M TMAO, 2.9 and 2.7 kcal $mol^{-1}$ $M^{-1}$, respectively. Therefore, it is reasonable to expect that if a mutation has very little effect on the urea *m* value, as seen in Table 2, then a similar lack of effect on the TMAO *m* value is likely.

### *H2A*

The $\Delta\Delta G°$(Ala–Gly) values indicate that helix propensity is a significant determinant of monomer stability, particularly for residues in α2 (Glu61, Glu64, and Asn68). Except for the helix cap residue (Asn89), all mutation sites exhibited ϕ(Ala–Gly) values of $\geq 0.7$, indicating that the stabilizing contribution of helix propensity is fully attained in the folding of the H2A monomer; additional contributions of these residues to dimer stability must arise from side-chain interactions.

In the H2A monomer, Glu61 and Glu91 appear to be folded, given that E61G and E91G are destabilizing; however, their ϕ Gly values of 0.3 to 0.4 (Table 3) indicate that their stabilizing potential is only partially fulfilled. These two residues are in the midst of a cluster of acidic residues that includes Glu56, Glu64, Asp90, Glu92, and Glu102. This acidic patch appears to interact with the highly basic H4 histone tails of adjacent nucleosomes in higher-order chromatin structure.[55] The enhanced stability of E61A suggests that components of this cluster are folded in the monomer, and removal of electrostatic repulsion is stabilizing. Conversely, E91A is WT-like in stability, consistent with its location at the edge of the cluster and proximity to Lys95. The WT-like stability of E64G indicates that this residue is presumably unfolded. An explanation for the very stabilizing effect of E64A is that the concomitant removal of electrostatic repulsion in formation of the acidic cluster and enhanced helix propensity induce propagation of the α2 helix that is folded around Glu61. Asn68 and Asn89 also appear to be largely unfolded, given the minimal effects of the Gly substitutions. However, N68A significantly enhances the free energy and cooperativity of unfolding [increased $\Delta G°(H_2O)$ and *m* values; Table 2], indicating that folding can be induced by increased helix propensity at the C-terminus of α2. A similar phenomenon is observed for other α2 Ala mutations (E61A and E64A): Ala substitutions significantly stabilize the H2A monomer but destabilize the heterodimer (or stabilize to a lesser extent for E64A). This observation is consistent with the suggestion that helix propensity/formation is a greater component of the monomer's stability than side-chain interactions; the dimer is destabilized because of a loss of favorable side-chain interactions that outweigh the stabilization derived from increased helix propensity. It is noted that Glu64 and Asn68 form intermolecular hydrogen bonds to His46 of H2B.

In summary, the mutations indicate that the central portion of α2 and the short αC helix are folded in the monomers and may interact, but there is minimal stabilization of the monomer contributed by the C-terminal regions of α2 and α3. Removal of potential electrostatic repulsion (E64A/G) or enhanced helix propensity (N68A) can induce further folding of the α2 helix in the H2A monomer.

### *H2B*

Lys43 in α1 appears in an unfolded region because of the lack of destabilization by K43G. However, K43A significantly stabilizes the H2B monomer while destabilizing the heterodimer. As described above, it appears that enhanced helix propensity can induce folding, but stabilizing interactions observed in the native dimer, such as the Lys43–Asp48 intramolecular salt bridge, are not present in the monomer.

Gly mutations at the three sites that span the α2 helix (Ser57, Asn64, and Glu73) are destabilizing, indicating that there is significant folding of the central helix in the monomer. However, similar to H2A, the ϕ Gly values indicate that the stabilizing interactions of these residues are only partially formed in the isolated monomer (Table 3). S57A and N64A have WT-like stability, despite the significant increase in helix propensity,[56] suggesting loss of stabilizing side-chain interactions in the monomer; similar effects are seen for dimer stability. At the C-terminal end of the α2 helix, Glu73 forms a local salt bridge with Arg76, which appears to be quite stabilizing; both Ala and Gly are destabilizing, with the largest $\Delta\Delta G°$ values of the monomer mutations in this study.

In summary, much of the α2 helix of H2B seems to be significantly folded in the isolated monomer, in contrast to H2A. In general, the ϕ(Ala–Gly) values for H2B are less than those for H2A, suggesting that side-chain interactions contribute to stability to a greater extent in H2B.

## Monomeric intermediates in the folding of helical dimers

Examples of dimeric proteins that fold via transient monomeric intermediates include malate dehydrogenase,[57] bacterial luciferase,[58–60] glutathione *S*-transferases,[16,61,62] and *E. coli* Trp repressor (TR).[8,9,63,64] It is most informative to compare the histone kinetic intermediates to those observed for other α-helical, domain-swapped dimers of comparable molecular weight, albeit different topologies, such as TR and the *E. coli* FIS (Factor for Inversion Stimulation).[65–67] In these three folds, most of the interactions in the hydrophobic core are formed by dimerization and intermolecular contacts; further-

more, these three dimers have virtually identical equilibrium $m$ values, suggesting that the total amount of surface area buried in the conversion of 2U to $N_2$ is comparable. The expected native fold of the isolated monomer should be relatively extended with a large solvent-accessible hydrophobic surface, particularly for the histone fold and the core dimerization motif of TR.[68–70]

The formation of a dimeric kinetic intermediate within 5 ms is a common feature of the eukaryotic histone heterodimers H2A–H2B[23] and H3–H4,[22] as well as the dimerization core of TR[69,70] and FIS,[66] and precluded determination of whether the dimerization-competent species were unfolded or partially folded monomers. Equilibrium studies of a Leu-to-Glu mutation in full-length TR[8,9] showed that the isolated TR monomers are highly helical, ~67% of the native dimer, and monomer folding buries ~60% of the solvent accessible surface area of $N_2$. The summed helical content of H2A and H2B (~60% of the native heterodimer) is comparable, but the histones have a greater buried surface area (70–85% of 2U to $N_2$). The temperature dependence of the folding kinetics of the TR dimerization core at submicromolar concentrations demonstrated that dimerization was entropically driven, presumably by gain of solvent entropy upon burial of hydrophobic surface area.[70] It was hypothesized that the efficiency of the nearly diffusion-limited association reaction could be the result of nonspecific interactions of exposed hydrophobic surfaces on partially folded monomeric species.[69] It will be of great interest to ascertain if the association of the histone monomers is also entropically driven, and the extent to which nonnative structure(s) impedes or accelerates the association reaction. Dimerization may be inhibited if an overly collapsed structure minimized exposed hydrophobic surface area and buried appropriate docking interfaces. However, nonnative structural components could accelerate dimerization by bringing together sufficient hydrophobic surface area to provide a large, nonspecific docking interface that could be easily rearranged in the conversion of $I_2$ to $N_2$ (Scheme 1).

### Conclusions

The isolated H2A and H2B monomers are partially folded with significant helical structure, buried surface area, and stability. The central α2 helix of the histone fold appears to be important for the stability of both monomers, and H2B is more folded and stable than H2A. Refolding of the isolated monomers to the native dimer demonstrates that the partially folded monomers are appropriate models for a monomeric kinetic species. However, the equilibrium data suggest that the isolated monomers adopt an overly collapsed conformation with presumably nonnative interactions. There is some indication of tertiary interactions between the α2 and αC helices of H2A. Such a structure would provide a docking surface for H2B, specifically the central portion of the α2 helix and the loop that connects the αC helix to the canonical histone fold. Further mutational studies are in progress to test this hypothesis.

## Materials and Methods

### Materials

Ultrapure urea was purchased from ICN Biomedicals (Costa Mesa, CA). TMAO solutions (Sigma-Aldrich, St. Louis, MO) were deionized with AG 11A8 Resin (Bio-Rad, Hercules, CA) and filter sterilized, and the concentration was determined by refractive index.[41] All other chemicals were of molecular biology or reagent grade from JT Baker (Phillipsburg, NJ).

### Methods

#### *Production of recombinant histone monomers*

H2A and H2B variants were constructed using four-way PCR methods,[71] and the entire histone genes were sequenced to confirm the presence of the desired substitutions and the lack of any other mutations. WT and mutant H2A and H2B monomers were overexpressed and purified from inclusion bodies as previously described.[40] The histone monomers were stored in 10 mM HCl and diluted into 200 mM KCl, 20 mM potassium phosphate (KPi; pH7.2), and 0.1 mM dipotassium ethylenediaminetetraacetic acid ($K_2$EDTA) for all equilibrium and kinetic experiments. HPLC SEC (Phenomenex, Biosep-SEC-S-2000) was used to determine the oligomeric state of histones under the different experimental conditions. Bovine serum albumin (66.4 kDa), ribonuclease A (13.7 kDa), myoglobin (17.0 kDa), and the H2A–H2B dimer (27.4 kDa) were used as molecular weight standards.

#### *Equilibrium and kinetic data collection*

Acrylamide quenching and equilibrium FL experiments were performed using an AVIV ATF-105/305 differential/ratio spectrofluorometer. Equilibrium CD, SF-CD, and SF-FL experiments were performed on an AVIV 202SF spectrophotometer. The CD and FL instruments were equipped with Hamilton Model 500 titrators for automated equilibrium experiments. An AVIV Instruments SF tower interfaced with the AVIV 202SF was used for the collection of kinetic data. Far-UV CD scans were collected with a 1-nm wavelength interval (symbols in Figs. 2b, 4a and c, and 5a are to identify the scans and do not represent all of the collected data). Urea was used to denature the histone monomers for direct comparison to the equilibrium parameters obtained previously for H2A–H2B.[38,40] Equilibration times during the titrations were 2 min at each urea concentration, significantly longer than kinetic relaxation times of the monomers, which fold and unfold within the SF burst phase, that is, <5 ms. CD data were collected at 222 nm. Intrinsic Tyr FL was monitored at 308 nm with excitation at 280 nm. SF-FL emission intensity was monitored at 90° relative to the incident light using a 295-nm cutoff filter. The dead time of the SF instrument was ~5 ms with flow rates of 2 ml/s. Multiple kinetic jumps were averaged, 30 and 20 traces for CD and FL, respectively, to improve the signal-to-noise ratio of the kinetic response.

*Data analysis*

Acrylamide quenching data were analyzed with KaleidaGraph 4.0 software (Synergy Software, Reading, PA) using the Stern–Volmer equation:

$$\frac{F_0}{F} = (1 + K_{SV}[Q])\exp(V[Q]) \quad (1)$$

where $F_0/F$ is the ratio of the FL intensities in the absence and presence of acrylamide, $Q$, and $K_{SV}$ and $V$ are the dynamic and static quenching constants, respectively.

The equilibrium unfolding transitions monitored by CD and FL for the isolated monomers were fit to a two-state model using Savuka 5.1.[2] The following well-established, linear relationship between free energy and urea concentration was used:

$$\Delta G^{\circ} = \Delta G^{\circ}(H_2O) + m[\text{Urea}] \quad (2)$$

where $\Delta G°(H_2O)$ is the free energy of unfolding in the absence of urea and the $m$ value describes the sensitivity of the transition to the urea concentration. $F_{app}$ is related to the observed spectral properties by the following relationship:

$$F_{app} = \frac{Y_i - Y_N}{Y_U - Y_N} \quad (3)$$

where $Y_i$ is the spectroscopic signal observed at $[\text{Urea}]_i$ and $Y_N$ and $Y_U$ are the spectral properties of the folded and unfolded baselines, respectively. However, even in 1 M TMAO, the native FL baselines were not readily defined in local fits because of their steep urea dependence. Thus, fitting was an iterative process. Initially, the FL data were fit with the $m$ value [Eq. (2)] fixed at the value determined from local fits of the CD equilibrium data. This constraint allowed a more precise definition of the native baselines. In subsequent local fits, the baseline parameters (slope and intercept) were then fixed at these values, and the $m$ values were treated as adjustable parameters to generate the most realistic local fits of the data. In global fits of the CD and FL data, the $\Delta G°(H_2O)$ and $m$ values were treated as global parameters across all equilibrium titrations for a given monomer, and the baselines were treated as local parameters. Reported errors represent one standard deviation of the error surface of the global fit as determined by rigorous error analyses.[46]

SF refolding was initiated by mixing isolated monomers that were pre-equilibrated at either 0 or 0.4 M urea concentrations with jumps to the same final urea concentration of 0.4 M. SF-CD and SF-FL refolding responses from the same initial conditions were fit locally and globally to a single, first-order exponential as done previously for H2A–H2B refolding from urea-unfolded monomers.[23] There was excellent agreement between the rates determined from local and global fits.


## Acknowledgements

This work was supported by a National Institute of General Medical Sciences grant (GM073787) to L.M.G. M.R.S. was partially supported by a National Institutes of Health Biotechnology training grant (GM08336).


## Supplementary Data

Supplementary data associated with this article can be found, in the online version, at doi:10.1016/j.jmb.2008.10.040

## References


1. Milla, M. E. & Sauer, R. T. (1994). P22 Arc repressor: folding kinetics of a single-domain, dimeric protein. *Biochemistry*, **33**, 1125–1133.
2. Zitzewitz, J. A., Bilsel, O., Luo, J., Jones, B. E. & Matthews, C. R. (1995). Probing the folding mechanism of a leucine zipper peptide by stopped-flow circular dichroism spectroscopy. *Biochemistry*, **34**, 12812–12819.
3. Sosnick, T. R., Jackson, S., Wilk, R. R., Englander, S. W. & DeGrado, W. F. (1996). The role of helix formation in the folding of a fully alpha-helical coiled coil. *Proteins*, **24**, 427–432.
4. Durr, E., Jelesarov, I. & Bosshard, H. R. (1999). Extremely fast folding of a very stable leucine zipper with a strengthened hydrophobic core and lacking electrostatic interactions between helices. *Biochemistry*, **38**, 870–880.
5. Jaenicke, R. & Lilie, H. (2000). Folding and association of oligomeric and multimeric proteins. *Adv. Protein Chem.* **53**, 329–401.
6. Fink, A. L. (1998). Protein aggregation: folding aggregates, inclusion bodies and amyloid. *Folding Des.* **3**, R9–R23.
7. Matthews, C. R. (1993). Pathways of protein folding. *Annu. Rev. Biochem.* **62**, 653–683.
8. Shao, X., Hensley, P. & Matthews, C. R. (1997). Construction and characterization of monomeric tryptophan repressor: a model for an early intermediate in the folding of a dimeric protein. *Biochemistry*, **36**, 9941–9949.
9. Shao, X. & Matthews, C. R. (1998). Single-tryptophan mutants of monomeric tryptophan repressor: optical spectroscopy reveals nonnative structure in a model for an early folding intermediate. *Biochemistry*, **37**, 7850–7858.
10. Eliezer, D., Chung, J., Dyson, H. J. & Wright, P. E. (2000). Native and non-native secondary structure and dynamics in the pH4 intermediate of apomyoglobin. *Biochemistry*, **39**, 2894–2901.
11. Spence, G. R., Capaldi, A. P. & Radford, S. E. (2004). Trapping the on-pathway folding intermediate of Im7 at equilibrium. *J. Mol. Biol.* **341**, 215–226.
12. Whittaker, S. B., Spence, G. R., Gunter Grossmann, J., Radford, S. E. & Moore, G. R. (2007). NMR analysis of the conformational properties of the trapped on-pathway folding intermediate of the bacterial immunity protein Im7. *J. Mol. Biol.* **366**, 1001–1015.
13. Gunasekaran, K., Eyles, S. J., Hagler, A. T. & Gierasch, L. M. (2001). Keeping it in the family: folding studies of related proteins. *Curr. Opin. Struct. Biol.* **11**, 83–93.
14. Zarrine-Afsar, A., Larson, S. M. & Davidson, A. R. (2005). The family feud: do proteins with similar structures fold via the same pathway? *Curr. Opin. Struct. Biol.* **15**, 42–49.
15. Alves, C. S., Kuhnert, D. C., Sayed, Y. & Dirr, H. W. (2006). The intersubunit lock-and-key motif in human glutathione transferase A1-1: role of the key residues Met51 and Phe52 in function and dimer stability. *Biochem. J.* **393**, 523–528.

16. Thompson, L. C., Walters, J., Burke, J., Parsons, J. F., Armstrong, R. N. & Dirr, H. W. (2006). Double mutation at the subunit interface of glutathione transferase rGSTM1-1 results in a stable, folded monomer. *Biochemistry*, **45**, 2267–2273.
17. Kim, D. H., Jang, D. S., Nam, G. H. & Choi, K. Y. (2001). Folding mechanism of ketosteroid isomerase from *Comamonas testosteroni*. *Biochemistry*, **40**, 5011–5017.
18. Kim, D. H., Nam, G. H., Jang, D. S., Yun, S., Choi, G., Lee, H. C. & Choi, K. Y. (2001). Roles of dimerization in folding and stability of ketosteroid isomerase from *Pseudomonas putida* biotype B. *Protein Sci.* **10**, 741–752.
19. Nam, G. H., Cha, S. S., Yun, Y. S., Oh, Y. H., Hong, B. H., Lee, H. S. & Choi, K. Y. (2003). The conserved *cis*-Pro39 residue plays a crucial role in the proper positioning of the catalytic base Asp38 in ketosteroid isomerase from *Comamonas testosteroni*. *Biochem. J.* **375**, 297–305.
20. Nam, G. H., Kim, D. H., Ha, N. C., Jang, D. S., Yun, Y. S., Hong, B. H. *et al.* (2003). Contribution of conserved amino acids at the dimeric interface to the conformational stability and the structural integrity of the active site in ketosteroid isomerase from *Pseudomonas putida* biotype B. *J. Biochem.* **134**, 101–110.
21. Topping, T. B. & Gloss, L. M. (2004). Stability and folding mechanism of mesophilic, thermophilic and hyperthermophilic archaeal histones: the importance of folding intermediates. *J. Mol. Biol.* **342**, 247–260.
22. Banks, D. D. & Gloss, L. M. (2004). Folding mechanism of the $(H3–H4)_2$ histone tetramer of the core nucleosome. *Protein Sci.* **13**, 1304–1316.
23. Placek, B. J. & Gloss, L. M. (2005). Three-state kinetic folding mechanism of the H2A/H2B histone heterodimer: the N-terminal tails affect the transition state between a dimeric intermediate and the native dimer. *J. Mol. Biol.* **345**, 827–836.
24. Baxevanis, A. D., Arents, G., Moudrianakis, E. N. & Landsman, D. (1995). A variety of DNA-binding and multimeric proteins contain the histone fold motif. *Nucleic Acids Res.* **23**, 2685–2691.
25. Xie, X., Kokubo, T., Cohen, S. L., Mirza, U., Hoffmann, A., Chait, B. T. *et al.* (1996). Structural similarity between TAFs and the heterotetrameric core of the histone octamer. *Nature*, **380**, 316–322.
26. Birck, C., Poch, O., Romier, C., Ruff, M., Mengus, G., Lavigne, A. C. *et al.* (1998). Human $TAF_{II}28$ and $TAF_{II}18$ interact through a histone fold encoded by atypical evolutionary conserved motifs also found in the SPT3 family. *Cell*, **94**, 239–249.
27. Selleck, W., Howley, R., Fang, Q., Podolny, V., Fried, M. G., Buratowski, S. & Tan, S. (2001). A histone fold TAF octamer within the yeast TFIID transcriptional coactivator. *Nat. Struct. Biol.* **8**, 695–700.
28. Davey, C. A., Sargent, D. F., Luger, K., Maeder, A. W. & Richmond, T. J. (2002). Solvent mediated interactions in the structure of the nucleosome core particle at 1.9 Å resolution. *J. Mol. Biol.* **319**, 1097–1113.
29. Luger, K., Mader, A. W., Richmond, R. K., Sargent, D. F. & Richmond, T. J. (1997). Crystal structure of the nucleosome core particle at 2.8 Å resolution. *Nature*, **389**, 251–260.
30. Zhu, W., Sandman, K., Lee, G. E., Reeve, J. N. & Summers, M. F. (1998). NMR structure and comparison of the archaeal histone HFoB from the mesophile *Methanobacterium formicicum* with HMfB from the hyperthermophile *Methanothermus fervidus*. *Biochemistry*, **37**, 10573–10580.
31. Decanniere, K., Babu, A. M., Sandman, K., Reeve, J. N. & Heinemann, U. (2000). Crystal structures of recombinant histones HMfA and HMfB from the hyperthermophilic archaeon *Methanothermus fervidus*. *J. Mol. Biol.* **303**, 35–47.
32. Stump, M. R. & Gloss, L. M. (2008). Unique fluorophores in the dimeric archaeal histones hMfB and hPyA1 reveal the impact of nonnative structure in a monomeric kinetic intermediate. *Protein Sci.* **17**, 322–332.
33. Isenberg, I. (1979). Histones. *Annu. Rev. Biochem.* **48**, 159–191.
34. D'Anna, J. A. & Isenberg, I. (1974). A histone cross-complexing pattern. *Biochemistry*, **13**, 4992–4997.
35. D'Anna, J. A., Jr & Isenberg, I. (1972). Fluorescence anisotropy and circular dichroism study of conformational changes in histone IIb2. *Biochemistry*, **11**, 4017–4025.
36. D'Anna, J. A., Jr & Isenberg, I. (1974). Conformational changes of histone LAK (f2a2). *Biochemistry*, **13**, 2093–2098.
37. Deleage, G. & Geourjon, C. (1993). An interactive graphic program for calculating the secondary structure content of proteins from circular dichroism spectrum. *Comput. Appl. Biosci.* **9**, 197–199.
38. Placek, B. J. & Gloss, L. M. (2002). The N-terminal tails of the H2A–H2B histones affect dimer structure and stability. *Biochemistry*, **41**, 14960–14968.
39. Munoz, V. & Serrano, L. (1997). Development of the multiple sequence approximation within the AGADIR model of alpha-helix formation: comparison with Zimm–Bragg and Lifson–Roig formalisms. *Biopolymers*, **41**, 495–509.
40. Gloss, L. M. & Placek, B. J. (2002). The effect of salts on the stability of the H2A–H2B histone dimer. *Biochemistry*, **41**, 14951–14959.
41. Wang, A. & Bolen, D. W. (1997). A naturally occurring protective system in urea-rich cells: mechanism of osmolyte protection of proteins against urea denaturation. *Biochemistry*, **36**, 9101–9108.
42. Bolen, D. W. & Baskakov, I. V. (2001). The osmophobic effect: natural selection of a thermodynamic force in protein folding. *J. Mol. Biol.* **310**, 955–963.
43. Henkels, C. H., Kurz, J. C., Fierke, C. A. & Oas, T. G. (2001). Linked folding and anion binding of the *Bacillus subtilis* ribonuclease P protein. *Biochemistry*, **40**, 2777–2789.
44. Banks, D. D. & Gloss, L. M. (2003). Equilibrium folding of the core histones: the H3–H4 tetramer is less stable than the H2A–H2B dimer. *Biochemistry*, **42**, 6827–6839.
45. Placek, B. J., Harrison, L. N., Villers, B. M. & Gloss, L. M. (2005). The H2A.Z/H2B dimer is unstable compared to the dimer containing the major H2A isoform. *Protein Sci.* **14**, 514–522.
46. Beechem, J. M. (1992). Global analysis of biochemical and biophysical data. *Methods Enzymol.* **210**, 37–54.
47. Myers, J. K., Pace, C. N. & Scholtz, J. M. (1995). Denaturant *m* values and heat capacity changes: relation to changes in accessible surface areas of protein folding. *Protein Sci.* **4**, 2138–2148.
48. Mello, C. C. & Barrick, D. (2003). Measuring the stability of partly folded proteins using TMAO. *Protein Sci.* **12**, 1522–1529.
49. Fersht, A. R. (1999). *Structure and mechanism in protein science: A guide to enzyme catalysis and protein folding*, W.H. Freeman & Co, New York.
50. Sanchez, I. E. & Kiefhaber, T. (2003). Origin of unusual phi-values in protein folding: evidence against specific nucleation sites. *J. Mol. Biol.* **334**, 1077–1085.
51. Fersht, A. R. & Sato, S. (2004). Phi-value analysis and

the nature of protein-folding transition states. *Proc. Natl Acad. Sci. USA*, **101**, 7976–7981.
52. Baskakov, I. & Bolen, D. W. (1998). Forcing thermodynamically unfolded proteins to fold. *J. Biol. Chem.* **273**, 4831–4834.
53. Bolen, D. W. & Rose, G. D. (2008). Structure and energetics of the hydrogen-bonded backbone in protein folding. *Annu. Rev. Biochem.* **77**, 339–362.
54. Gursky, O. (1999). Probing the conformation of a human apolipoprotein C-1 by amino acid substitutions and trimethylamine-*N*-oxide. *Protein Sci.* **8**, 2055–2064.
55. Suto, R. K., Clarkson, M. J., Tremethick, D. J. & Luger, K. (2000). Crystal structure of a nucleosome core particle containing the variant histone H2A.Z. *Nat. Struct. Biol.* **7**, 1121–1124.
56. Pace, C. N. & Scholtz, J. M. (1998). A helix propensity scale based on experimental studies of peptides and proteins. *Biophys. J.* **75**, 422–427.
57. Rudolph, R., Fuchs, I. & Jaenicke, R. (1986). Reassociation of dimeric cytoplasmic malate dehydrogenase is determined by slow and very slow folding reactions. *Biochemistry*, **25**, 1662–1669.
58. Clark, A. C., Raso, S. W., Sinclair, J. F., Ziegler, M. M., Chaffotte, A. F. & Baldwin, T. O. (1997). Kinetic mechanism of luciferase subunit folding and assembly. *Biochemistry*, **36**, 1891–1899.
59. Apuy, J. L., Park, Z. Y., Swartz, P. D., Dangott, L. J., Russell, D. H. & Baldwin, T. O. (2001). Pulsed-alkylation mass spectrometry for the study of protein folding and dynamics: development and application to the study of a folding/unfolding intermediate of bacterial luciferase. *Biochemistry*, **40**, 15153–15163.
60. Noland, B. W. & Baldwin, T. O. (2003). Demonstration of two independently folding domains in the alpha subunit of bacterial luciferase by preferential ligand binding-induced stabilization. *Biochemistry*, **42**, 3105–3112.
61. Wallace, L. A. & Dirr, H. W. (1999). Folding and assembly of dimeric human glutathione transferase A1-1. *Biochemistry*, **38**, 16686–16694.
62. Hornby, J. A., Luo, J. K., Stevens, J. M., Wallace, L. A., Kaplan, W., Armstrong, R. N. & Dirr, H. W. (2000). Equilibrium folding of dimeric class mu glutathione transferases involves a stable monomeric intermediate. *Biochemistry*, **39**, 12336–12344.
63. Mann, C. J. & Matthews, C. R. (1993). Structure and stability of an early folding intermediate of *Escherichia coli* trp aporepressor measured by far-UV stopped-flow circular dichroism and 8-anilino-1-naphthalene sulfonate binding. *Biochemistry*, **32**, 5282–5290.
64. Gloss, L. M., Simler, B. R. & Matthews, C. R. (2001). Rough energy landscapes in protein folding: dimeric *E. coli* Trp repressor folds through three parallel channels. *J. Mol. Biol.* **312**, 1121–1134.
65. Hobart, S. A., Meinhold, D. W., Osuna, R. & Colon, W. (2002). From two-state to three-state: the effect of the P61A mutation on the dynamics and stability of the factor for inversion stimulation in an altered equilibrium denaturation mechanism. *Biochemistry*, **41**, 13744–13754.
66. Topping, T. B., Hoch, D. A. & Gloss, L. M. (2004). Folding mechanism of FIS, the intertwined, dimeric factor for inversion stimulation. *J. Mol. Biol.* **335**, 1065–1081.
67. Meinhold, D., Boswell, S. & Colon, W. (2005). P61A mutation in the factor for inversion stimulation results in a thermostable dimeric intermediate. *Biochemistry*, **44**, 14715–14724.
68. Gloss, L. M. & Matthews, C. R. (1997). Urea and thermal equilibrium denaturation studies on the dimerization domain of *Escherichia coli Trp* repressor. *Biochemistry*, **36**, 5612–5623.
69. Gloss, L. M. & Matthews, C. R. (1998). Mechanism of folding of the dimeric core domain of *Escherichia coli Trp* repressor: a nearly diffusion-limited reaction leads to the formation of an on-pathway dimeric intermediate. *Biochemistry*, **37**, 15990–15999.
70. Gloss, L. M. & Matthews, C. R. (1998). The barriers in the biomolecular and unimolecular folding reaction of the dimeric core domain of *Escherichia coli Trp* repressor are dominated by enthalpic contributions. *Biochemistry*, **37**, 16000–16010.
71. Ho, S. N., Hunt, H. D., Horton, R. M., Pullen, J. K. & Pease, L. R. (1989). Site-directed mutagenesis by overlap extension using the polymerase chain reaction. *Gene*, **77**, 51–59.